

Received 29 December 2023; revised 31 January 2024 and 5 February 2024; accepted 14 February 2024. Date of publication 16 February 2024;
date of current version 1 March 2024. The review of this article was arranged by Editor G. I. Ng.

Digital Object Identifier 10.1109/JEDS.2024.3366804

Improving the Manufacturability of Low-Temperature GaN Ohmic Contact by Blocking the Fluorine Ion Injection

TONG LIU, XIANGDONG LI (Member, IEEE), ZHANFEI HAN, LILI ZHAI, JUNBO WANG, SHUZHEN YOU[✉],
JINCHENG ZHANG[✉] (Member, IEEE), JIE ZHANG, ZHIBO CHENG, YUANHANG ZHANG,
QIUSHUANG LI, AND YUE HAO[✉] (Senior Member, IEEE)

Guangzhou Wide Bandgap Semiconductor Innovation Center, Guangzhou Institute of Technology, Xidian University, Guangzhou 510555, China

CORRESPONDING AUTHORS: X. LI AND J. ZHANG (e-mail: xdli@xidian.edu.cn; jchzhang@xidian.edu.cn)

This work was supported by the National Key Research and Development Program of China under Grant 2021YFB3600900.

ABSTRACT Stabilizing the CMOS-compatible low-temperature Au-free GaN Ohmic contact is a critical work that determines the performance and yield of GaN power HEMTs in mass production. The instability of this contact has been puzzling the industry and academia for years. In this work, an overlooked factor, fluorine injection, is unambiguously verified to widely exist during dielectric etching and can easily destroy the low-temperature GaN Ohmic contact formation. The injection depth is confirmed to be over 30 nm with a fluorine peak concentration of 10^{23} at/cm³ in vicinity of the surface. Traditional method of partial AlGaN recessing with a pretty tiny processing window is proven unfriendly for production and vulnerable to the fluorine injection. Two methods to get rid of the fluorine are proposed. The first one is to over-etch the AlGaN barrier to the GaN channel to fully remove the fluorine ions. The second is to deposit an etch-stop blocking layer of Al₂O₃, which is also compatible with CMOS process.

INDEX TERMS GaN, HEMT, Ohmic contacts, low-temperature, fluorine injection.

I. INTRODUCTION

GaN HEMTs offers great perspectives for high-performance power devices for many applications such as renewable energy, industrial electronics, and electric vehicles, thanks to the high electron mobility, high critical electric field, and high frequency [1], [2], [3], [4], [5], [6], although most GaN power devices are today still employed in consumer electronics. To date, several aspects that hinder the widespread applications of GaN HEMTs still exists, for instance, the relatively high cost, low yield, and non-formalized reliability and processing.

To lower the cost and promote mass production, high-productivity CMOS-compatible and Au-free process is indispensable. However, most eminent source/drain metallization schemes are based on Au-containing metal stacks assisted by rapid thermal annealing (RTA) under a very high temperature of above 800 °C [7], [8], [9]. This is anyway unsuitable because of the high cost. Thus, some other techniques, for instance, Ti/Al/Ni/TiN [10], Ti/Al [11],

Ti/Al/W [12], and TiAl alloy [13] are proposed. Low Ohmic contact resistance R_C of $< 1 \Omega \cdot \text{mm}$ can be obtained at the risk of high annealing temperature, which is harmful to the self-aligned gate-first process and the passivation dielectrics [14]. Plus, high-temperature treatment may also trigger some reliability problems [15], [16].

Low-temperature metallization scheme is then achieved by Ta/Al metal stack that is unfortunately not compatible with CMOS process [17]. Further optimized Au-free low-temperature metallization scheme is thus proposed, which focuses on the widely used Ti/Al stack in microelectronics industry. It is believed that plenty of donor-like N vacancies in AlGaN or GaN can be generated so that to form the Ohmic contact [18], [19]. Firincieli et al. found that the Ti/Al ratio of 0.05 is crucial to reduce R_C of the Au-free low-temperature Ti/Al/TiN contact to $0.62 \pm 0.06 \Omega \cdot \text{mm}$ [20]. Pre-ohmic recess etching of AlGaN barrier [21], [22] was also proven effective to reduce the R_C . However, the strict thickness of the residual AlGaN barrier leads to a pretty

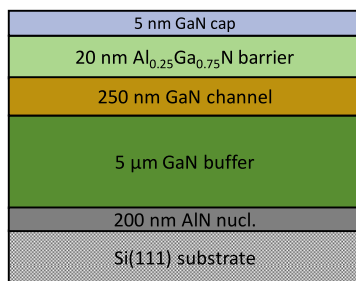


FIGURE 1. Schematic cross-sectional view of the AlGaN/GaN heterostructure on the Si(111) substrate.

small processing window, which is not applicable for mass production. Moreover, Wang et al. pointed out, during the Ohmic contact window opening, the fluorine-based plasma etching of dielectric on top of the AlGaN can degrade the Ohmic contact by injecting the fluorine ions to the dielectric and AlGaN barrier [23]. Therefore, to boost the yield of the low-temperature Au-free GaN Ohmic contact for mass production, the impact of fluorine injection and AlGaN etching requires in-depth investigation.

In this work, we report on the impact of the fluorine injection on the low-temperature Au-free GaN Ohmic contact. At the beginning, the traditional Ohmic contact window is opened by fluorine-based reactive ion etching (RIE) on the SiO₂/AlGaN to illustrate the existence of imperfect Ohmic contact by this method. Then, RIE etching on the blanket AlGaN surface is conducted to prove the existence of fluorine injection. Later, two methods of AlGaN over-etching and Al₂O₃ etch-stop layer deposition are proposed to effectively block the fluorine injection and improve the quality and yield of the low-temperature Au-free GaN Ohmic contact for mass production.

II. EXPERIMENTS

The AlGaN/GaN heterostructure wafer used in this paper was grown on a 6-inch Si substrate by metal organic chemical vapor deposition system (MOCVD). The epitaxy stack consists of 5 nm GaN cap layer, 20 nm Al_{0.25}Ga_{0.75}N barrier layer, 250 nm GaN channel layer, ~5 μm GaN buffer layer, and 200 nm AlN nucleation layer, from top to bottom, as shown in Fig. 1. Hall mobility and 2DEG sheet resistance of the AlGaN/GaN heterostructure reach 1800 cm²/V·s and 380 Ω/□, respectively.

200 nm SiO₂ was first deposited on the GaN wafer using plasma enhanced chemical vapor deposition (PECVD) to passivate the top surface. Then the Ohmic contact windows were patterned by lithography, after which the SiO₂ was etched off by CHF₃-based RIE with an etching rate of about 22 nm/min. Afterwards, part of the AlGaN barrier layer was recessed by BC_l₃/Cl₂-based inductively coupled plasma (ICP) dry etching, and the power of the ICP source and RF generator were set to 150 and 25 W, respectively, with a BC_l₃/Cl₂ flow rate of 8/20 sccm and a pressure of 20 mTorr. The etching rate is tuned to as low as 0.9

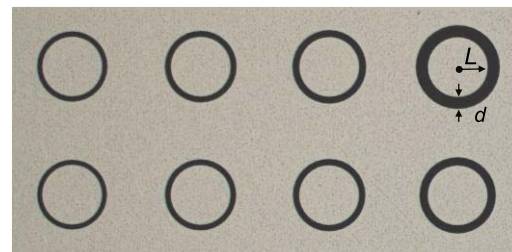


FIGURE 2. Photograph of the fabricated CTLM test structure.

TABLE 1. Summary of the processed samples in this work.

Sample	structure	process	Ohmic contact?
A10		10-min RIE+25-s ICP	No
A11	SiO ₂ /GaN/AlGaN/GaN	11-min RIE+25-s ICP	No
A12		12-min RIE+25-s ICP	No
B0		0-min RIE+25-s ICP	Yes
B2	GaN/AlGaN/GaN	2-min RIE+25-s ICP	No
B4		4-min RIE+25-s ICP	No
C20		12-min RIE+20-s ICP	No
C25	SiO ₂ /GaN/AlGaN/GaN	12-min RIE+25-s ICP	No
C40		12-min RIE+40-s ICP	Yes
D5	SiO ₂ /Al ₂ O ₃ /GaN/AlGaN/GaN	12-min RIE+ wet +25-s ICP	Yes

nm/s. Notably, to investigate the impact of RIE and ICP, various etching time and depth were investigated. Next, the photoresist was stripped and the samples were subjected to a wet treatment in 18% HCl to remove the surface oxides. Finally, Ti/Al (10 nm/200 nm) was deposited using e-beam evaporation as the Ohmic contact metal, followed by a final RTA for 60 s at 550 °C in the ambient of N₂. All samples have the same epitaxial structure and fabrication process, except for variations in passivation stack, RIE and ICP etching time. Detailed sample structure and processing flow are summarized in TABLE 1. The microstructures of the samples were characterized using scanning electron microscopy (SEM) and transmission electron microscopy (TEM).

After fabrication, the Ohmic contacts were subjected to electrical characterization with a circular transmission line model (CTLM) by Keysight B1500A, where the test structure is plotted in Fig. 2. In order to eliminate the parasitic effect of probe resistance, a four-point probe method was adopted for current testing.

III. RESULTS

A. IMPACT OF RIE OVER-ETCHING ON OHMIC CONTACT

In reality, certain level of over-etching of SiO₂ or other passivation dielectric layer is always obligatory due to the inhomogeneity of the dielectric thickness and RIE etching. Therefore, the first group of comparative experiments come with etching the same 200 nm SiO₂ with three different RIE

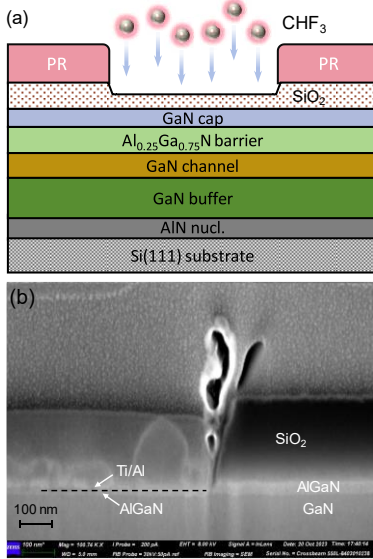


FIGURE 3. (a) Schematic structure of sample A10, A11, and A12, and (b) SEM image of sample A10 with 10-min RIE etching on the SiO₂ and subsequent 25-s AlGaN recessing by ICP.

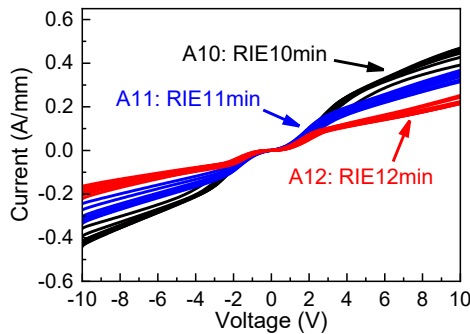


FIGURE 4. I-V characteristics of the sample A10, A11, and A12, corresponding to RIE etching of the 200 nm SiO₂ for 10, 11, and 12 minutes and subsequent 25-s AlGaN recessing by ICP.

etching time of 10, 11, and 12 minutes, corresponding to the over-etching time of about 1, 2, and 3 minutes, respectively, as shown in Fig. 3(a). The AlGaN barrier layer was then partially recessed for 25 s by ICP, leading to a ~2.5 nm AlGaN barrier layer retained, as shown by the SEM image in Fig. 3(b). These three samples are denoted as sample A10, A11, and A12. Fig. 4 demonstrates the I-V characteristics of the fabricated CTLM on the three samples. Schottky but not Ohmic contacts are formed, and the drain current decreases with the RIE over-etching time, indicating the RIE etching can probably damage the Ohmic contact.

B. VERIFICATION OF THE FLUORINE INJECTION

In order to mitigate the possible interference by the SiO₂ dielectric itself, we further conducted RIE etching on the blanket GaN wafer without any dielectric on top for 0, 2, and 4 minutes, followed by the subsequent 25-s AlGaN recessing, metal evaporation, and RTA. These three samples are denoted as sample B0, B2, and B4. Fig. 5 illustrates

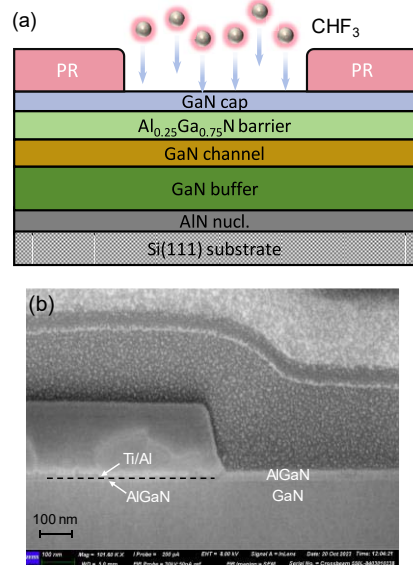


FIGURE 5. (a) Schematic structure of sample B0, B2 and B4, and (b) SEM image of sample B0 without RIE etching, but with 25-s AlGaN recessing by ICP.

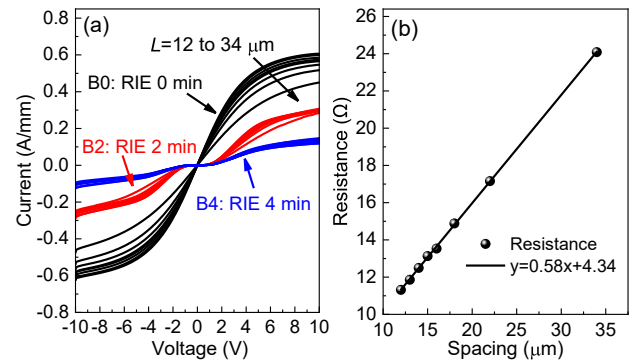


FIGURE 6. (a) I-V characteristics of the sample B0, B2, and B4 corresponding to the RIE etching time of 0, 2, and 4 minutes on the blanket GaN wafer, and subsequent 25-s AlGaN recessing by ICP, and (b) linear fitting of total resistance versus spacing of sample B0.

the microstructure of sample B0, where pretty satisfactory Ohmic contacts are formed with a high current density of 624 mA/mm, R_C of 1.29 Ω·cm, and ρ_c of 4.83×10^{-5} Ω·cm⁻², as shown in Fig. 6. Obviously, the current keeps on degrading from 624 to 283, and finally to 132 mA/mm as the RIE etching time increases from 0 to 4 minutes. This clear trend unambiguously proves that the RIE over-etching does jeopardize the Ohmic contact formation.

To further verify the existence of fluorine ions in the epitaxial layer, secondary ion mass spectroscopy (SIMS) profiles of the fluorine were then probed as shown in Fig. 7. The fluorine peak concentration reaches 3×10^{22} at/cm³ after RIE etching of 4 minutes. A potential barrier is therefore lifted up between the metal and the AlGaN barrier, thus destroying the Ohmic contact formation [23].

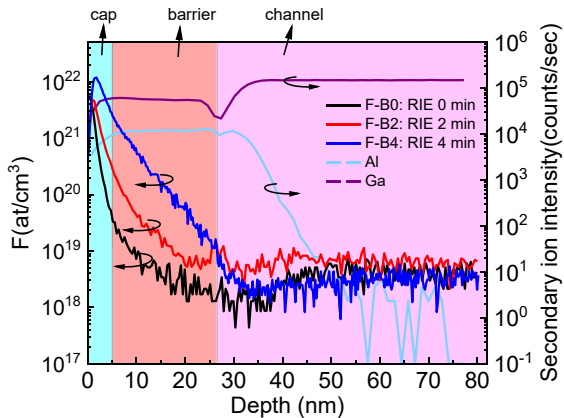


FIGURE 7. SIMS distribution profiles of the fluorine ions in the epitaxial layer induced by RIE etching of sample B0, B2, and B4, and distribution profiles of Al and Ga.

C. SUPPRESSING THE IMPACT OF FLUORINE INJECTION BY ALGAN RECESSING

Next, solutions to mitigate the drawback of fluorine injection during RIE etching is proposed. The first method is to physically remove these ions by recessing the AlGaN barrier and even the GaN channel with ICP etching. After opening the Ohmic contact window by RIE etching of the 200 nm SiO₂ for 12 minutes, AlGaN/GaN recessing by ICP etching was then performed for 20, 25, and 40 seconds, corresponding to etching depth of 18, 22.5, and 36 nm, as shown in Fig. 8(a). These three samples are denoted as sample C20, C25, and C40, respectively.

TEM images in Fig. 8(b)-(d) depict the detailed recessed AlGaN/GaN heterostructures after various ICP etching. Over-etching of the GaN channel of Sample C40 can be clearly observed, which may more thoroughly remove the fluorine. From Fig. 9(a) we can see the current does improve with the ICP etching time, indicating the Ohmic contact can be indeed restored by over-recessing the AlGaN barrier. The Ohmic contact parameters extracted from Fig. 9(b) shows sample C40 features a R_C of 1.05 Ω·cm and ρ_c of 3.48×10^{-5} Ω·cm⁻². According to the SIMS profile in Fig. 7, it can be easily concluded that the impact of fluorine injection can be sufficiently removed by over-recessing the AlGaN barrier.

D. SUPPRESSING THE IMPACT OF FLUORINE INJECTION BY AN ETCH-STOP BLOCKING LAYER

It is also noticed that some other teams favor the non-recessed [24] or partially-recessed [22] low-temperature Ohmic contact. Therefore, another 5-nm Al₂O₃ etch-stop layer is proposed here to block the fluorine injection. In this experiment, the 5-nm Al₂O₃ was first deposited by plasma-enhanced atomic layer deposition (PEALD) on the GaN wafer, denoted as sample D5, followed by 200 nm SiO₂ deposition and then RIE etching for 12 minutes with an over-etching time of ~ 3 minutes. Before the Ohmic metal Ti/Al deposition, hydrochloric acid wet etching was employed to remove the Al₂O₃ and 25-s AlGaN recessing by ICP, as shown in Fig. 10(a). The microstructure of the

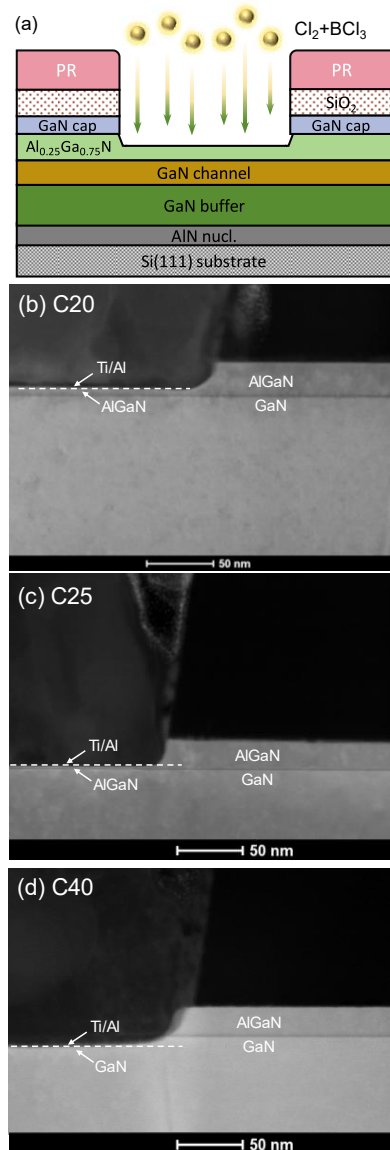


FIGURE 8. (a) Schematic structure of sample C20, C25, and C40, and TEM images of the contact structures of sample (b) C20, (c) C25, and (d) C40 with different ICP etching time of 20 s, 25 s, and 40 s, respectively.

sample D5 was checked by the SEM image in Fig. 10(b), where the Al₂O₃/SiO₂ passivation stack can be observed. R_C of 1.45 Ω·cm and ρ_c of 6.27×10^{-5} Ω·cm⁻² are achieved for sample D5 with the 5-nm Al₂O₃ etch-stop blocking layer, as shown in Fig. 11.

IV. DISCUSSION

Temperature-dependent *I-V* characteristics of the sample A11 with 11-min RIE etching and subsequent 25-s AlGaN recessing are plotted in Fig. 12(a). The *I-V* curves are clearly divided into two parts by a point of intersection. That is, from 0 to 2 V, the current increases with the temperature due to the thermally enhanced field emission [23]; from 2 V, the current drops due to the mobility degradation at higher temperatures. This phenomenon is basic for the Schottky barrier diode [25], indicating that a potential barrier has been

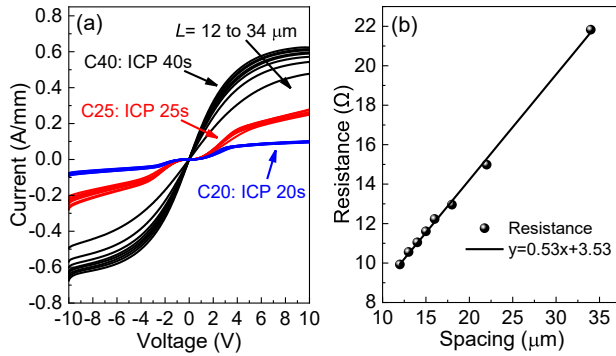


FIGURE 9. (a) I-V characteristics of the sample C20, C25, and C40 after ICP etching for 20 s, 25 s, and 40 s, respectively, and (b) linear fitting of total resistance versus spacing of sample C40.

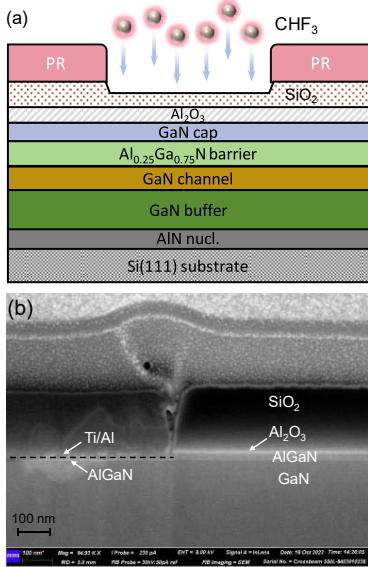


FIGURE 10. (a) Schematic structure and (b) SEM image of sample D5 with 12-min RIE etching on the SiO₂, wet etching of the Al₂O₃, and subsequent 25-s AlGaN recessing by ICP.

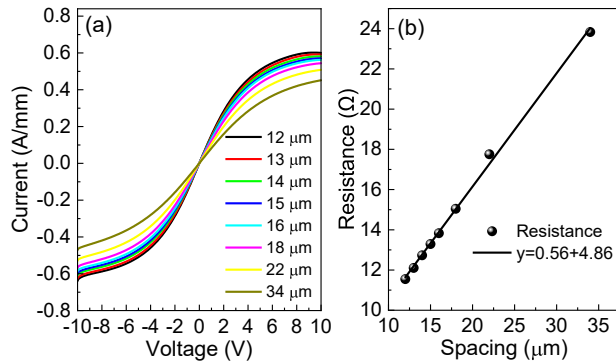


FIGURE 11. (a) I-V characteristics of the sample D5 with 5-nm Al₂O₃ after 12-min RIE etching on the SiO₂, wet etching of the Al₂O₃, and subsequent 25-s AlGaN recessing by ICP, and (b) linear fitting of total resistance versus spacing for sample D5.

formed by the fluorine injection. Identical characteristics have also been found in sample B2 and sample C25 as shown in Fig. 12(b) and (c).

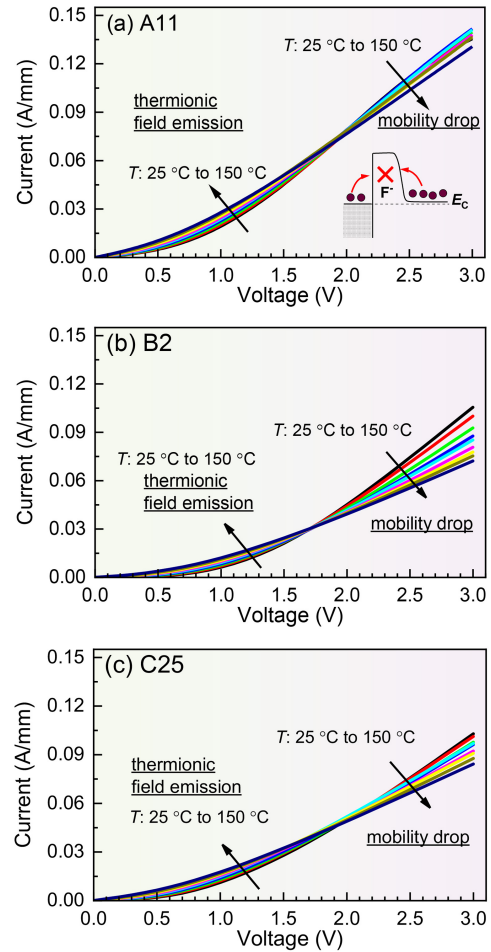


FIGURE 12. Temperature-dependent I-V characteristics of (a) sample A11, (b) sample B2, and (c) sample C25.

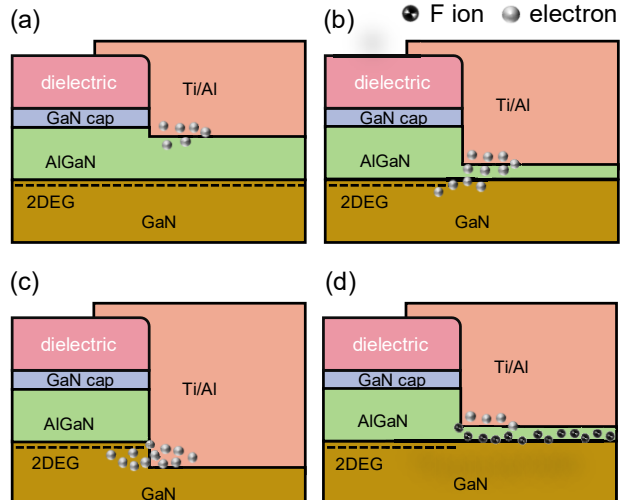


FIGURE 13. Schematic contact mechanisms of (a) insufficient recessing, (b) moderate recessing, and (c) over-recessing of AlGaN barrier, and (d) fluorine injection that blocks the carrier transport.

The schematic contact mechanisms and the influence of fluorine injection are depicted in Fig. 13. The residual AlGaN thickness after recessing is crucial. As seen from

Fig. 13(a) to (c), the key to guarantee the formation of Ohmic contact is to ensure the distance between the contact metal and the 2DEG. Previous works have claimed to retain part of the AlGaN barrier to keep the 2DEG under the contact metal, so as to give a better contact. This method is difficult to be employed in mass production because the strict thickness results in a pretty tiny processing window. Moreover, this Ohmic contact can be destroyed by the fluorine injection as shown in Fig. 13(d), where the detailed mechanism is plotted by the inset of Fig. 12. Therefore, over-recessing is more practical, where the 2DEG can be connected to the metal through the side wall as in Fig. 13(c). Even if the contact suffers the fluorine injection, over-etching can easily etch off these negative ions, which is exactly the case of sample C40.

V. CONCLUSION

Impact of fluorine injection on the CMOS-compatible low-temperature Au-free GaN Ohmic contact has been explored in this work. The existence and drawback of fluorine injection during the Ohmic contact window opening by RIE etching are unambiguously verified. Two effective methods to suppress this impact were proposed. The first is to fully recess the AlGaN barrier even to the GaN channel layer to physically remove the injected fluorine. The second method is to deposit a Al_2O_3 etch-stop blocking layer to fully block the fluorine injection from the root. These two methods are both compatible with the mass production of GaN HEMTs. Moreover, the confirmation of the fluorine injection successfully explains the long-standing puzzle of the terrible repeatability of GaN low-temperature Ohmic contact, which is of great significance for boosting the manufacturability of GaN power HEMTs.

REFERENCES

- [1] H. Amano et al., "The 2018 GaN power electronics roadmap," *J. Phys. D, Appl.*, vol. 51, no. 16, Mar. 2018, Art. no. 163001, doi: [10.1088/1361-6463/aaaf9d](https://doi.org/10.1088/1361-6463/aaaf9d).
- [2] K. J. Chen et al., "GaN-on-Si power technology: Devices and applications," *IEEE Trans. Electron Devices*, vol. 64, no. 3, pp. 779–795, Mar. 2017, doi: [10.1109/TED.2017.2657579](https://doi.org/10.1109/TED.2017.2657579).
- [3] H. Wang et al., "Investigation of thermally induced threshold voltage shift in normally-OFF p-GaN gate HEMTs," *IEEE Trans. Electron Devices*, vol. 69, no. 5, pp. 2287–2292, May 2022, doi: [10.1109/TED.2022.3157805](https://doi.org/10.1109/TED.2022.3157805).
- [4] C. Sun, Z. Niu, and S. Yang, "Dynamic gate capacitance model for switching transient analysis in P-GaN gate HEMTs," in *Proc. 35th Int. Symp. Power Semicond. Devices ICs (ISPSD)*, 2023, pp. 291–294, doi: [10.1109/ISPSD57135.2023.10147460](https://doi.org/10.1109/ISPSD57135.2023.10147460).
- [5] R. Gao et al., "Towards understanding the interaction between hydrogen poisoning and bias stress in AlGaN/GaN MIS-HEMTs with SiN_x gate dielectric," *IEEE Electron Device Lett.*, vol. 42, no. 2, pp. 212–215, Feb. 2021, doi: [10.1109/LED.2021.3049245](https://doi.org/10.1109/LED.2021.3049245).
- [6] C. Pan et al., "Physical mechanism of device degradation & its recovery dynamics of p-GaN gate HEMTs under repetitive short circuit stress," in *Proc. IEEE 34th Int. Symp. Power Semicond. Devices ICs (ISPSD)*, 2022, pp. 313–316, doi: [10.1109/ISPSD49238.2022.9813685](https://doi.org/10.1109/ISPSD49238.2022.9813685).
- [7] X. Yang et al., "Low specific contact resistivity of $10^{-3} \Omega\cdot\text{cm}^2$ for Ti/Al/Ni/Au multilayer metals on Si-GaN: Fe substrate," *IEEE Trans. Electron Devices*, vol. 69, no. 10, pp. 5773–5779, Oct. 2022, doi: [10.1109/TED.2022.3201784](https://doi.org/10.1109/TED.2022.3201784).
- [8] Z. Fan, S. N. Mohammad, W. Kim, Ö. Aktas, A. E. Botchkarev, and H. Morkoç, "Very low resistance multilayer ohmic contact on GaN," *Appl. Phys. Lett.*, vol. 68, no. 12, pp. 1672–1674, Mar. 1996, doi: [10.1063/1.115901](https://doi.org/10.1063/1.115901).
- [9] S. Ruvimov et al., "Microstructure of Ti/Al and Ti/Al/Ni/Au ohmic contacts for n-GaN," *Appl. Phys. Lett.*, vol. 69, no. 11, pp. 1556–1558, Sep. 1996, doi: [10.1063/1.117060](https://doi.org/10.1063/1.117060).
- [10] X. Li, S. Gao, Q. Zhou, X. Liu, W. Hu, and H. Wang, "Fabrication and performance of Ti/Al/Ni/TiN Au-free ohmic contacts for undoped AlGaN/GaN HEMT," *IEEE Trans. Electron Devices*, vol. 67, no. 5, 282 pp. 1959–1964, May 2020, doi: [10.1109/TED.2020.2982665](https://doi.org/10.1109/TED.2020.2982665).
- [11] M. E. Lin, Z. Ma, F. Y. Huang, Z. F. Fan, L. H. Allen, and H. Morkoc, "Low resistance ohmic contacts on wide band-gap GaN," *Appl. Phys. Lett.*, vol. 64, no. 8, pp. 1003–1005, 1994, doi: [10.1063/1.111961](https://doi.org/10.1063/1.111961).
- [12] H.-S. Lee, D. S. Lee, and T. Palacios, "AlGaN/GaN high-electron-mobility transistors fabricated through a Au-free technology," *IEEE Electron Device Lett.*, vol. 32, no. 5, pp. 623–625, May 2011, doi: [10.1109/LED.2011.2114322](https://doi.org/10.1109/LED.2011.2114322).
- [13] M. Y. Fan et al., "Ultra-low contact resistivity of ultra-low contact resistivity of $<0.1 \Omega\cdot\text{mm}$ for Au-Free Ti_xAl_y Alloy contact on non-recessed i-AlGaN/GaN," *IEEE Electron Device Lett.*, vol. 41, no. 1, pp. 143–146, Jan. 2020, doi: [10.1109/LED.2019.2953077](https://doi.org/10.1109/LED.2019.2953077).
- [14] M. Piazza, C. Dua, M. Oualli, E. Morvan, D. Carisetti, and F. Wyczisk, "Degradation of TiAlNiAu as ohmic contact metal for GaN HEMTs," *Microelectron. Rel.*, vol. 49, nos. 9–11, pp. 1222–1225, Sep. 2009, doi: [10.1016/j.microrel.2009.06.043](https://doi.org/10.1016/j.microrel.2009.06.043).
- [15] T. Hashizume and H. Hasegawa, "Effects of nitrogen deficiency on electronic properties of AlGaN surfaces subjected to thermal and plasma processes," *Appl. Surf. Sci.*, vol. 234, nos. 1–4, pp. 387–394, Jul. 2004.
- [16] S. Huang et al., "Effects of interface oxidation on the transport behavior of the two-dimensional-electron-gas in AlGaN/GaN heterostructures by plasma-enhanced-atomic-layer-deposited AlN passivation," *J. Appl. Phys.*, vol. 114, no. 14, Oct. 2013, Art. no. 144509.
- [17] A. Malmros, H. Blanck, and N. Rorsman, "Electrical properties, microstructure, and thermal stability of Ta-based ohmic contacts annealed at low temperature for GaN HEMTs," *Semicond. Sci. Tech. nol.*, vol. 26, no. 7, Mar. 2011, Art. no. 075006, doi: [10.1088/0268-1242/26/7/075006](https://doi.org/10.1088/0268-1242/26/7/075006).
- [18] B. P. Luther, S. E. Mohney, T. N. Jackson, M. A. Khan, Q. Chen, and J. W. Yang, "Investigation of the mechanism for ohmic contact formation in Al and Ti/Al contacts to n-type GaN," *Appl. Phys. Lett.*, vol. 70, no. 1, pp. 57–59, Jan. 1997, doi: [10.1063/1.119305](https://doi.org/10.1063/1.119305).
- [19] A. Shriki et al., "Formation mechanism of gold-based and gold-free ohmic contacts to AlGaN/GaN heterostructure field effect transistors," *J. Appl. Phys.*, vol. 121, no. 6, 2017, Art. no. 065301, doi: [10.1063/1.4975473](https://doi.org/10.1063/1.4975473).
- [20] A. Firincieli, B. De Jaeger, S. You, D. Wellekens, M. Van Hove, and S. Decoutere, "Au-free low temperature ohmic contacts for AlGaN/GaN power devices on 200 mm Si substrates," *Jpn. J. Appl. Phys.*, vol. 53, no. 4S, Jan. 2014, Art. no. 04EF01, doi: [10.7567/Jpn.53.53.04ef01](https://doi.org/10.7567/Jpn.53.53.04ef01).
- [21] J. Zhang et al., "Mechanism of Ti/Al/Ti/W Au-free ohmic contacts to AlGaN/GaN heterostructures via pre-ohmic recess etching and low temperature annealing," *Appl. Phys. Lett.*, vol. 107, no. 26, pp. 1–6, 2015, doi: [10.1063/1.4939190](https://doi.org/10.1063/1.4939190).
- [22] J. Zhang et al., "Ultralow-contact-resistance Au-free ohmic contacts with low annealing temperature on AlGaN/GaN heterostructures," *IEEE Electron Device Lett.*, vol. 39, no. 6, pp. 847–850, Jun. 2018, doi: [10.1109/LED.2018.2822659](https://doi.org/10.1109/LED.2018.2822659).
- [23] Y. Wang et al., "Effects of fluorine plasma treatment on Au-free ohmic contacts to ultrathin-barrier AlGaN/GaN heterostructure," *IEEE Trans. Electron Devices*, vol. 66, no. 7, pp. 2932–2936, Jul. 2019, doi: [10.1109/TED.2019.2916997](https://doi.org/10.1109/TED.2019.2916997).
- [24] A. Constant et al., "Impact of Ti/Al atomic ratio on the formation mechanism of non-recessed Au-free ohmic contacts on AlGaN/GaN heterostructures," *J. Appl. Phys.*, vol. 120, no. 10, 2016, Art. no. 104502, doi: [10.1063/1.4962314](https://doi.org/10.1063/1.4962314).
- [25] T. Zhang et al., "A 1.9-kV/2.61-m $\Omega\cdot\text{cm}^2$ lateral GaN Schottky barrier diode on silicon substrate with tungsten anode and low Turn-ON voltage of 0.35 V," *IEEE Electron Device Lett.*, vol. 39, no. 10, pp. 1548–1551, Oct. 2018, doi: [10.1109/LED.2018.2864874](https://doi.org/10.1109/LED.2018.2864874).